Faculty
Engineering

The optimal hydraulic diameter of semicircular and triangular shaped channels for compact heat exchangers.

J.C. Venter (B.Eng)

Mini dissertation submitted in partial fulfillment of the degree
Magister of Engineering
at the
Postgraduate School of Nuclear Science and Engineering,
of the
North-West University

Supervisor: Dr. Jan-Hendrik Kruger

November 2010

NORTH-WEST UNIVERSITY
UNIBESITI YA BOKONE-BOPHIRIMA
NOORDWES-UNIVERSITEIT
POTCHEFSTROOMKAMPUS

Abstract

Title : The optimum hydraulic diameter of semicircular and triangular shaped channels for compact heat exchangers.

Author : J.C. Venter

Supervisor : Dr. JH Kruger

School : Postgraduate School of Nuclear Science and Engineering

Degree : Masters of Engineering

All heat pump cycles have one common feature that connects them to one another; this feature is the presence of a heat exchanger. There are even some heat-driven cycles that are completely composed of heat exchangers, every heat exchanger fulfilling a different, though critical role.

The need therefore exists to optimize heat exchangers, more specifically Compact Heat Exchangers (CHE). This study deals with the optimization of such a CHE by determining an optimal hydraulic diameter of the micro-channels in a CHE, for minimal hydraulic losses. Two Computational Fluid Dynamics (CFD) models were developed for a single micro-channel that is present in a CHE. The first model had a semi-circular cross-section, the second a triangular cross-section.

The results were verified by comparing it with existing experimental data. Following the verification of the results, the micro-channel was optimized by implementing an optimum diameter for the lowest pressure drop over the micro-channel. This was done for both the semi-circular and triangular micro-channel cross-sections.

Keywords:
Micro heat exchangers, semicircular channel, triangular channel, hydrualic diameter, Nusselt number, pressure drop, micro channels, heat transfer, trapezoidal, straight.

Acknowledgements

Thank you Lord Jesus Christ, my Saviour, for leading, guiding and supporting me throughout this study.

Thank you, Claudia, my beautiful wife, for your love and support.

Thank you to Prof Jat du Toit, for valuable insight when it was needed most.

Thank you Dr. Jan-Hendrik Kruger for guidance during my dissertation.

I would like to give a special thanks to NRF and THRIP for funding, during my masters studies and for this project, without the funding it would not have been possible to do a postgraduate degree at the North-West University.

Table of contents

List of symbols

Symbol	Unit	Description
A	m	Half amplitude
A_s	m^2	Surface area
B	m	Trapezoidal step length
b	m	Perpendicular height of equilateral triangle
Ca	-	Capillary number
Cp	$J.kg^{-1}.K^{-1}$	Specific heat capacity at constant pressure
CS	-	Control surface
CV	-	Control volume
d	m	Channel diameter
e	J	Energy
e_f	-	Pressure drop penalty
e_{Nu}	-	Heat transfer enhancement
f_D	-	Darcy friction factor
$f_{straight}$	Pa	Pressure difference over a straight channel
$f_{trapezoidal}$	Pa	Pressure difference over a trapezoidal channel
D_h	m	Hydraulic diameter
H_{ave}	m	Average wall spacing
H_{max}	m	Maximum wall spacing
H_{min}	m	Minimum wall spacing
k	$W.m^{-1}.K^{-1}$	Thermal conductivity
L	m	Half wavelength
L_{hy}	m	Hydraulic entrance length
L_{th}	m	Thermal entrance length
Nu	-	Nusselt number
$Nu_{straight}$	-	Nusselt number in a straight channel
$Nu_{trapezoidal}$	-	Nusselt number in a trapezoidal channel
Nu_x	-	Nusselt number at specific axial location
Δp	Pa	Pressure difference
p	Pa	Pressure
p_{in}	Pa	Inlet pressure
p_{out}	Pa	Outlet pressure
$p_{x,y}$	Pa	Pressure at a point (x,y)
Pr		Prandtl number
q_w	$W.m^{-2}$	Wall heat flux
$\dot{Q}_{net\ in}$	Watt	Rate of energy
r_0	m	Radius
R_c	m	Radius of curvature
Re		Reynolds number
Re_d	-	Reynolds number as function of hydraulic diameter
Straight	-	Straight micro channel
Trapezoidal	-	Trapezoidal shaped micro channel
t	s	Time
T_w	K	Wall temperature
T_b	K	Bulk temperature
u(r)	m	Velocity as function of radius
$\forall$	m^3	Volume
$\dot{W}_{net\ in}$	Watt	Rate of work

Greek Symbols

λ	m	Wavelength
Φ	degrees	Phase angle
μ	$kg.s^{-1}.m^{-1}$	Dynamic viscosity
ρ	$kg.m^{-3}$	Density

List of accronyms

CFD	Computational fluid dynamics
CHE	Compact heat exchanger
DBHE	Diffusion bonded heat exchanger
HE	Heat exchanger
NRF	National Research Foundation
PCHE	Printed circuit heat exchanger
PFHE	Plate-fin heat exchanger
PHE	Plate heat exchanger
S&THX	Shell and tube heat exchanger
THRIP	Technology and Human Resources for Industry Programme

List of figures

List of tables

1. Introduction

Heat exchangers are used in many different engineering applications such as space heating and air-conditioning, waste heat recovery, chemical processing and power production. The main function of a heat exchanger is to exchange heat between two fluid streams which are at different temperatures and separated by a solid wall.

Despite the fact that there are various kinds of heat exchangers, each one fulfils the same role namely: transferring heat between fluids. Below is a list of common heat exchangers that are currently being used in the industry:

- Concentric tube heat exchangers (parallel or counter flow)
- Cross-flow heat exchangers (finned or unfinned)
- Shell-and-tube heat exchangers
- Compact heat exchangers

In this study the focus will be on the last type of heat exchanger mentioned above, which is the Compact heat exchanger (CHE) which can also be referred to as a micro heat exchanger. A heat exchanger can only be categorised as being a CHE when the hydraulic diameter (D_h) of the channel in which the fluid flows is smaller than 3mm. The hydraulic diameter can be seen as an 'effective' diameter that is used in internal flow calculations, were the cross-sectional flow area is not a conventional circular shape.

When installing a heat exchanger for a specific application the main objective is to transfer as much heat as possible from the fluid with the higher temperature to the fluid with the lower temperature. There are a couple of factors that influence the amount of heat that can be transferred; one of them being the area density. The area density of a heat exchanger is the ratio of heat transfer surface to the heat exchanger volume. The following graph in Fig. 1 (Reay, 2002:462), shows the different types of heat exchangers with the hydraulic diameter and area densities.

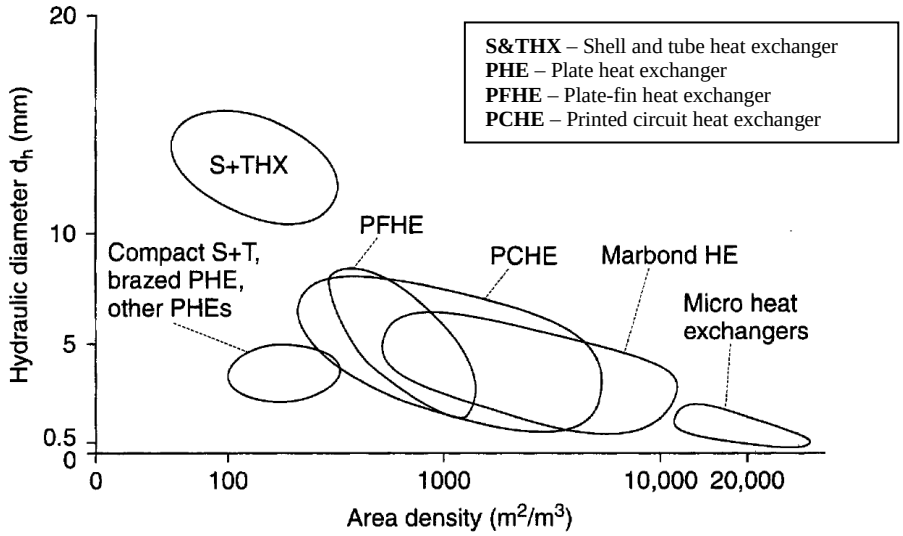

Figure 1 - Heat exchanger area densities and hydraulic diameters (Reay, 2002:462)

Comparing the different types of heat exchangers regarding their hydraulic diameter and area density, the micro heat exchangers top the scales in terms of size and volume, in the far right corner of Figure 1, with the highest area density and the lowest hydraulic diameter.

The following list of benefits goes hand in hand with the use of CHEs instead of the more conventional heat exchangers.

- Higher efficiency - A higher coefficient of performance is the result of the closer approach temperature to the heat pump.
- Installation costs are lower due to the smaller physical size of a CHE, less piping is the major fund saver,
- In absorption cycles multi-stream and multi-pass configurations can be easily applied when using CHE.
- The total thermal-hydraulic inertia of the system is lower giving the operator quicker response to operator changes when controlling the plant.
- A smaller fluid inventory makes the CHE a lot safer, especially when working with ammonia or hydrocarbons.
- The temperature and pressure limits of the cycle will not be determined by the heat exchanger, due to the fact that it can withstand high temperatures and pressures.

In the group of micro heat exchangers there are also various types of micro heat exchangers namely:

- Plate-fin heat exchanger
- Welded plate heat exchangers
- Plate and frame heat exchangers
- Compact shell and tube heat exchangers
- The Marbond heat exchanger
- Printed circuit heat exchanger
- Spiral heat exchanger
- Diffusion bonded heat exchanger

The specific type of CHE that was investigated in this study is called a diffusion-bonded heat exchanger (DBHE) and is internationally manufactured by Heatric Ltd. that forms part of a bigger company called Meggitt. The DBHE is manufactured by diffusion welding multiple layers of alloy sheets on top of each other. The result is a big heat exchanger core that contains well-defined passages forming the heat transfer and flow channels.

The lower pressure loss in the flow channels of the CHE is also a major contributor to the efficiency of the CHE. The pressure loss is a function of the hydraulic diameter, which in turn is a function of the geometrical dimensions of the cross-section of the channel. When altering the geometrical dimensions of the channel layout one changes the hydraulic performance of the channel, this phenomena was thoroughly investigated by Haller et al. (2009:2678). In the aforementioned study single L-bends were under investigation, whereas in the current study one unit of the trapezoidal channel has four consecutive L-bends, with a total bend angle of more than 90°.

In a study done by Gupta et al. (2008:2925) the following cross-sections were investigated: circular, semicircular, triangular and square. The results showed that the most promising cross-sections (in terms of hydraulic performance) are semicircular and triangular, each one having different benefits in its own right. Building on that research the current study has investigated the possibility of optimising the hydraulic performance of those two specific cross-sections.

In chapter 2 a literature survey was done on the different types of channels that were analyzed in various studies. A way of quantifying the heat transfer and pressure drop was discussed. The different boundary conditions, fully developed flow and hydraulic diameter were also investigated.

In chapter 3 the solution methodology for the straight and trapezoidal channels are discussed. The straight channel simulation models were verified by comparing the Nusselt numbers with the Nusselt number for fully developed flow in the semicircular and triangular cross-sections. The trapezoidal channel simulation models were verified by comparing the results with the results obtained from literature.

In chapter 4 the results of the trapezoidal channels were presented and discussed.

In chapter 5 the conclusions of this study are stated and recommendations are made for further study regarding this particular subject.

2. Literature Survey

2.1. Developed simulation geometries

In simulation models for fully developed laminar flow in micro-channels numerous features can be altered, e.g. the bend radius, channel path length, the channel shape and cross-section. A literature survey was done on previously developed simulation models that used different geometries in their analyses. Simple micro-channel, sinusoidal, trapezoidal and serpentine channels were investigated.

2.1.1. Micro channel

Simulating the fluid flow in the micro-channels of a CHE is not a new feat, an investigation regarding the fluid behaviour in micro-channels was done by Haller et al. (2009:2678) where the pressure loss and heat transfer in bending and branching micro-channels for various Reynolds (Re) numbers ranging from 10-3000 were calculated. When the flow channel of the fluid was split or redirected a better heat transfer coefficient was observed but with an inevitable increase in pressure loss. T-junctions and L-bends were used in the simulation of the fluid flow and heat transfer in the micro-channels. The simulation tool that was used in the study is CFDACE+2006. The channel elements that were simulated are shown in Figure 2.

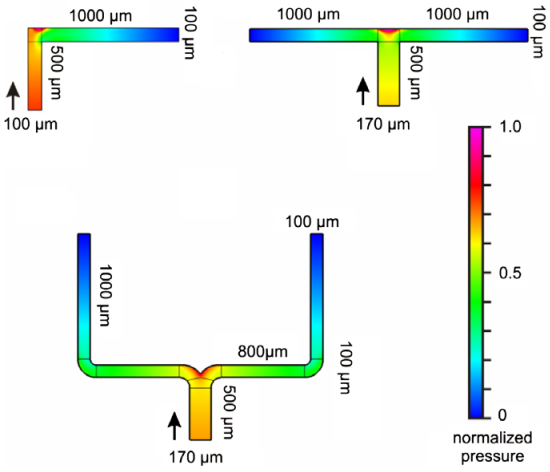

Figure 2 – Simulated channel elements from Haller et al. (2009:2678)

The heat transfer and pressure loss were found to be significantly influenced by the layout of the bends that were investigated. To get an impression of the physical behavior of the fluid in small elements was the aim of their study, in order to implement it in liquid cooling systems to achieve higher cooling ability and higher effectiveness.

It can be seen that the dimensions of these micro heat exchanger channels are much smaller than the conventional shell and tube heat exchanger tubes. Therefore the flow characteristics in micro channels are much different from that of the flow in standard sized tubes or ducts. The laws that govern flow in standard sized tubes are still present in micro channels but due to the small scale of micro channels small alterations in the geometry has much larger consequences, as can be seen in the experimental study that was done by Rosengarten et al. (2006:4169). In that study the effect of the contact angle on the liquid convection heat transfer in micro-channels was analyzed. An assumption was made that there exists a no-slip boundary condition at the wall. This particular assumption was in fact a very realistic one, due to its dependence on the wall shear stress of the channel. In that study it was shown that presence of slip, for a constant pressure, increases the Nusselt (Nu) number. By using thin film coating technology the surface wetability angle was modified between 20° and 120°. It was found that the contact angle and the wall shear rate can influence the heat transfer by up to 10%.

An interesting study was done by Gupta et al. (2009:2941) where Taylor-flow, also known as slug flow, in micro-channels were simulated in the Computational Fluid Dynamic (CFD) software package ANSYS. In that study it was concluded that because the liquid film surrounding the Taylor bubble in the micro-channel is very thin at low Capillary (Ca) numbers, the exact modeling of this phenomena should be done very carefully. To capture this incredibly thin film the mesh in the CFD model had to be very fine; the results however were in good agreement with previous modeling studies and existing correlations. That study clarified the role that the wall contact angle play in Taylor bubbling fluid flow situations.

Developing a numerical tool in order to simulate heat transfer and micro-channel flow was done in a study by Imke (2004:295). A forced convection body approach

combined with flow closure correlations in conventional pipes was the basis of the method that Imke (2004:295) used. The technique that he proposed may provide a fast and efficient tool for CFD simulation developers to estimate thermodynamic behavior that is dependent on operating conditions and the channel geometry. The program they developed can calculate vapor volume fractions, pressure losses, outlet temperatures and the thermo hydraulic conditions inside the heat exchanger when boiling occurs in the channels.

All of the studies that have been mentioned thus far, have focused on the behavior of the fluid due to a set of boundary conditions, while the work done by Haller et al. (2009:2678) only touched the surface of the fluid characteristics that can be observed due to geometrical channel alterations. This prompts a closer look at how heat transfer can be optimised by implementing geometrical modifications. The shape of the flow channel plays a significant role in the development of the flow in the channel and two specific channel shapes are of interest, the sinusoidal and trapezoidal channel shapes.

2.1.2. Sinusoidal channel simulations

Sinusoidally shaped channels were investigated by Rosaguti et al. (2007a:694). The shape of a sinusoidal channel can be seen in Figure 3. In the figure the symbols L, A and d represent the channel half wavelelength, amplitude and diameter respectively.

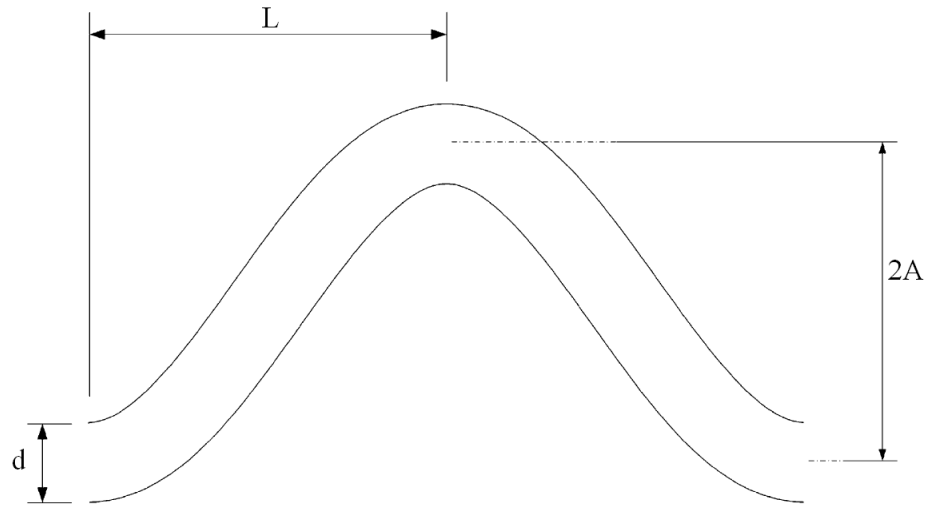

Figure 3 - Repeating module of a sinusoidal channel

In their study they report the effect of varying the Reynolds number ($5 \leq Re \leq 200$) and the non-dimensional relationships ($0.222 \leq A/L \leq 0.667$, $L/d = 4.5$) on the fully developed flow and heat transfer in a sinusoidal channel. The two boundary conditions[1] that were employed were the H2 boundary condition and T boundary condition. They concluded that the flow field in the sinusoidal channel is dominated by Dean's vortices[2] being formed as the Reynolds number and A/L relationship increase. Dean's vortices enhance convection heat transfer, with only a slight increase in the pressure drop over the sinusoidal channel compared to the pressure drop over a straight channel.

Another study was done by Rush et al. (1999:1541) on the heat transfer and pressure drop over sinusoidal wavy passages. The passages can be seen in Figure 4, note that the changing parameters in their study were the wave amplitude (A), phase angle (Φ), average wall to wall spacing (H_{ave}), maximum wall to wall spacing (H_{max}), minimum wall to wall spacing (H_{min}) and wavelength (λ).

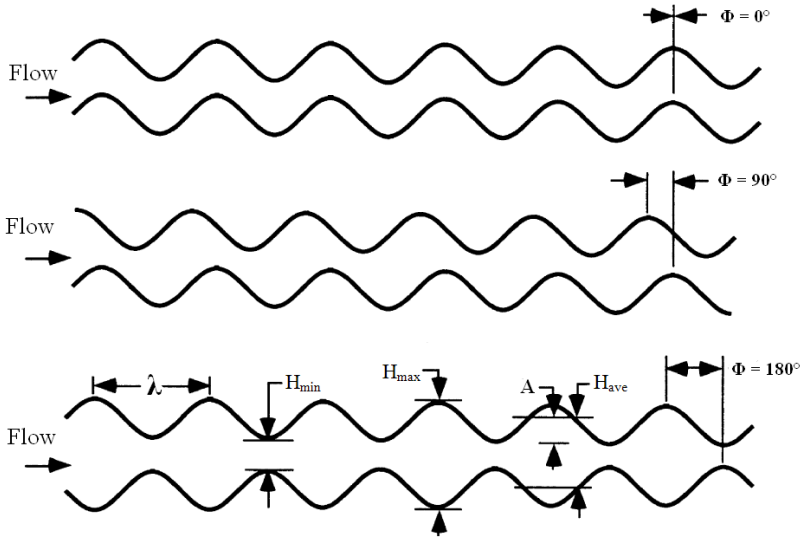

Figure 4 - Schematic of wavy passage from Rush, et al. (1999:1541)

The following table shows the values of which changing parameters for each experiment.

[1]The boundary conditions that can be applied to channels will be discussed thoroughly in section 2.3.
[2] Symmetric counter-rotating vortices.

Table 1- Flow visualization geometric parameters from Rush et al. (1999)

H_{min}	λ/H_{min}	A/H_{min}	Φ (degrees)
12.0	5.6	0.48	180
13.3	5.4	0.47	0
12.4	5.5	0.51	90
11.5	4.8	0.53	180
13.6	4.7	0.47	0
10.3	4.9	0.52	90
23.5	2.4	0.26	180
22.0	2.5	0.26	0
24.0	2.3	0.24	90
23.6	2.9	0.25	180
24.0	2.9	0.25	0
25.0	2.9	0.24	90

In the study of Rush et al. (1999:1541) the flow remained steady throughout the channel at very low Reynolds numbers, but at critical Reynolds numbers (dependent on phase shift and geometric parameters) the flow became unsteady and mixed at a distance equal to a wavelength from the end of the channel. As the Reynolds number increased the position where the mixing started moved closer to the inlet. Resulting that at high Reynolds numbers the mixing occurred within the first wavelength of the channel.

2.1.3. Trapezoidal channel simulations

CFD models were developed by Geyer et al. (2007) to study the heat transfer behavior of fully developed laminar flow. Trapezoidal channels with a semi-circular cross-section were simulated; Figure 5 shows the geometry of such a channel. In this figure the symbols are defined by the following: half wavelength (L), cross-section diameter (d), bend radius (R_c), trapezoidal step length (B) and half amplitude (A).

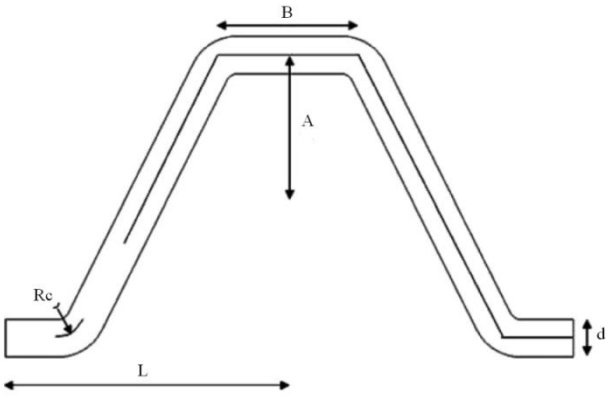

Figure 5 - Trapezoidal unit dimensions (Geyer et al. 2007)

Geyer et al. (2007) implemented constant wall heat flux (H2), constant axial heat flux with peripherally constant temperature (H1) and constant wall temperature (T) with a Prandtl number of 6.13 and a Reynolds number of up to 400. Their results confirmed that higher heat transfer rates are achieved with a relative small pressure drop penalty compared to a straight channel with the same active flow length.

The thermohydraulic performance of a periodic trapezoidal channel with a triangular cross-section was investigated by Gupta et al. (2008). They compared their results with trapezoidal channels that follows the same serpentine path but has a different cross-section namely square, circular and semicircular. The triangular and semicircular cross-sections were found to have the smallest pressure drop penalty compared with a straight channel.

2.1.4. Serpentine channel simulations

The serpentine channel is a combination of a sinusoidal and a trapezoidal channel, it can be seen in Figure 6. In the figure L, R_c and d represent the channel half-wavelength, bend radius and diameter respectively.

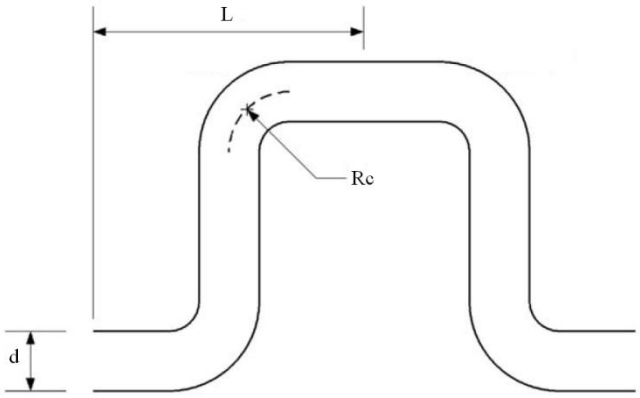

Figure 6 - Serpentine channel unit

The fully developed flow conditions in serpentine channels were investigated by Rosaguti et al. (2006:2912), using a semicircular cross-section. Rosaguti et al. (2006) used the following geometric configurations $3 < L/d < 12.5$, $0.525 < R_c/d < 2.25$ at a Reynolds number of 110. In the study it was observed that complex vertical flow patterns developed following the increase of the Reynolds number and the flow domain became increasingly dominated by these vortices. High rates of heat transfer occured because of the efficient fluid mixing caused by these vortices in the flow

domain. These vortices decayed downstream of the bends (Rosaguti et al. (2005:353)) but with the increase in Reynolds number the decay of the vortices in the flow channel were delayed.

2.1.5. Simulation Geometries Conclusion

After investigating a number of channel geometries that can be implemented in a compact heat exchanger the following conclusion can be made. Inserting bends in a channel increases the heat transfer but also increases the pressure drop over the channel. In the following section a method by which these characteristics can be quantified will be explained.

2.2. Quantifying the heat transfer and pressure drop

Assessing the performance of the channel in terms of heat transfer and pressure drop, the results obtained for the channels are compared with the values for fully developed flow in straight channels that has the same path length and diameter (Rosaguti et al. (2005:353)). To define the measure of heat transfer enhancement, a variable e_{Nu} is defined:

$$e_{Nu} = \frac{Nu_{trapezoidal}}{Nu_{straight}} \tag{1}$$

The $Nu_{trapezoidal}$ and $Nu_{straight}$ are the Nusselt numbers of a trapezoidal and a straight channel respectively, each having the same path length and diameter. Rosaguti et al. (2007:694) used the same measure of heat transfer variable but only substituting the Nusselt number for the trapezoidal channel with the Nusselt number that was calculated in that study, namely the Nusselt number for a serpentine channel.

Defining a measure of pressure drop, e_f, different parameters of the channels were used based on the same methodology as above, leading to:

$$e_f = \frac{(p_{in} - p_{out})_{trapezoidal}}{(p_{in} - p_{out})_{straight}} = \frac{f_{trapezoidal}}{f_{straight}} \tag{2}$$

The pressure drop over a trapezoidal channel $f_{trapezoidal}$ is compared with the pressure drop over a straight channel $f_{straight}$ (Gupta et al., 2007:3471). Where the p_{in} and p_{out} are the pressures averaged over the area at the inlet and the outlet respectively. The pressures are calculated using Eq. (3) from Rosaguti et al. (2005:353).

$$p = \frac{1}{A_s} \int_{A_s} p_{x,y} \, dA \tag{3}$$

2.3. Boundary Conditions

In order to solve any of the governing equations involved in simulation models one needs to specify the boundary conditions. The boundary conditions tailor the general equations to different flow and heat transfer situations. The uniqueness of one solution is usually dependent on the boundary conditions for which the numerical calculation is solved (Munson et al. 2007:750).

Ideal approximations for the boundary conditions that can be found in numerous practical applications are summarized in Table 2.

Table 2 - Thermal boundary conditions for developed flows through ducts (Shah & London, 1978:20)

Symbol	Description	Applications
T	Constant wall temperature; peripherally as well as axially	Condensers, evaporators, automotive radiators (at high flows), with negligible wall thermal resistance
T3	Constant axial wall temperature with finite normal wall resistance	Condensers, evaporators, automotive radiators (at high flows), with negligible wall thermal resistance
T4	Non-linear radiant-flux	Radiators in space power systems, high temperature liquid-metal facilities, high-temperature gas flow systems
H1	Constant axial wall heat flux with constant peripheral wall temperature	Highly conductive materials, electric resistance heating, nuclear heating, gas turbine regenerator
H2	Constant axial wall heat flux with uniform peripheral wall heat flux	Low conductive materials, duct with uniform wall thickness
H3	Constant axial wall heat flux with finite normal wall thermal resistance	Finite wall thermal resistance and negligible wall heat conduction

Of all the boundary conditions, the most often used in the simulation of micro-channels are the T, H1 and H2 boundary conditions. Implementing the H1 boundary condition in CFD simulations of heat transfer in swept passages was done by Rosaguti et al. (2007b:1833). Table 3 is a summary of the types of boundary conditions used in various studies.

Table 3 - List of studies and boundary conditions that were employed in each study

Reference	Boundary Condition
Geyer et al. (2007:3471)	T, H1, H2
Haller et al. (2009:2678)	T
Gupta et al. (2008:2925)	H2
Rosaguti et al. (2005:353)	H2
Rosaguti et al. (2006:2912)	T, H2
Rosaguti et al. (2007a:694)	T, H2
Rosengarten et al. (2006:4161)	H2
Rush et al. (1999:1541)	H2
Pei-Xue et al. (2001:1039)	H2

2.4. Fully developed flow

According to Shah & London (1978:35) there are two types of fully developed flows that can occur in any flow regime: thermally fully developed and hydro-dynamically fully developed flow. Only when the flow regime fulfils both sets of the conditions for thermal and hydraulic fully developed flow, can it be classified as fully developed flow. The flow regimes are not strongly linked to each other, so the flow can be fully developed thermally but still developing hydro-dynamically and vice versa. In Figures 7 and 8 the hydro-dynamically fully developed and thermally fully developed flow are illustrated. In Figure 7 the arrows represent the velocity magnitude, in the direction of the flow. In order to get the correct Nusselt number values the laminar flow regime of the fluid in the channel should be fully developed thermally and hydro-dynamically.

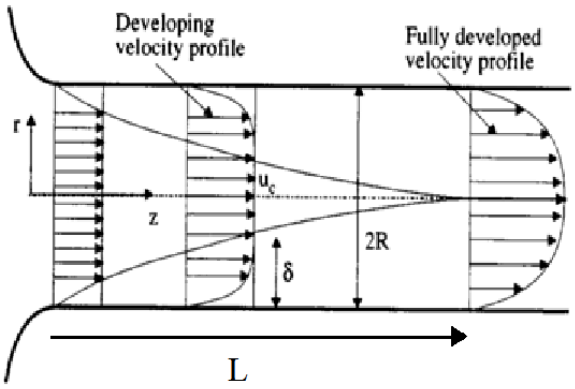

Figure 7 - Hydraulic fully developed flow (Kreith & Boehm, 1999)

Hydro-dynamically fully developed flow can be seen as the region in the flow where the velocity profile of the flow has reached dynamic equilibrium. The velocity profile of the fluid is then independent of the axial distance measured from the entrance of the duct to the fully developed region. The entrance length, L, from Figure 7 is a function of mainly two variables according to Shah and London (1978) and that is the Reynolds number and the hydraulic diameter.

From Incropera & De Witt (2005:469) the velocity profile in the flow through a circular duct is represented by the following parabolic function:

$$u(r)= -\frac{1}{4\mu}\left(\frac{dp}{dx}\right) r_0^2 \left[1-\left(\frac{r}{r_0}\right)^2\right] \tag{4}$$

As can be seen from Eq. 4 the velocity profile is dependent on the pressure gradient $\left(\frac{dp}{dx}\right)$ in the x-direction and the dynamic viscosity (μ) of the fluid. From Kreith & Boehm (1999:4-47) the length at which the the internal flow becomes hydrodynamic fully developed can be determined by

$$L_{hy}=0.0565 Re_d D_h \tag{5}$$

Where Re_d and D_h represent the Reynolds number and hydraulic diameter respectively.

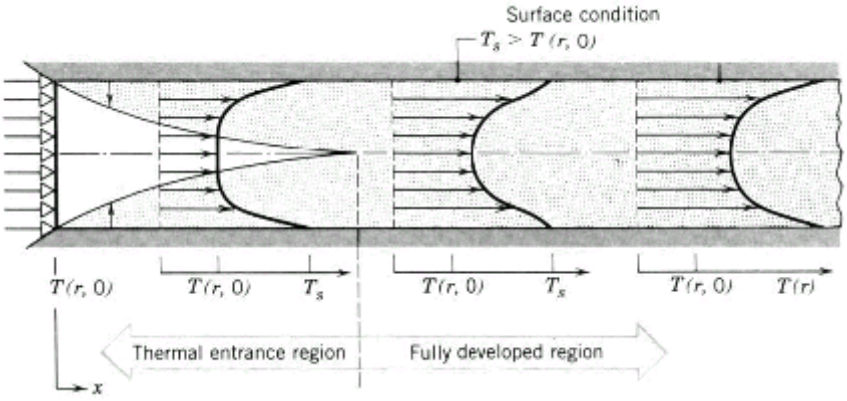

Figure 8 - Thermal fully developed flow (Incropera & De Witt (2005:472))

In Figure 8 the wall temperature (T_s) is higher than the inlet temperature of the fluid in the duct, thus forming a parabola in the direction opposite to that of the flow. From Kreith & Boehm (1999:4-47) the entry length ($L_{th,T}$) for thermally fully developed flow is represented by Eq, with the Prandtl number represented by Pr

$$L_{th,T}=0.037Re_dPrD_h \tag{6}$$

for the unifrom wall temperature boundary condition (T). If the uniform wall heat flux boundary condition is used the following equation from From Kreith & Boehm (1999:4-47) represents the thermal entry length ($L_{th,H2}$).

$$L_{th,H2}=0.053Re_dPrD_h \tag{7}$$

When comparing Eqns. (5) to (7) it is evident, that if Pr > 1, the hydro-dynamic entry length will be less than the thermal entry length, but for fluids with a *Pr* < 1, the inverse is true. When concidering a fluid with Pr > 100, such as some oils, the hydrodynamic entry length is much smaller than the thermal entry length. (Incropera & De Witt (2005:472))

2.5. Hydraulic diameter

The hydraulic diameter for a circular cross-section can be defined as the diameter of the circle. For a semicircle the hydraulic diameter is defined by Eq. (8) from Hesselgreaves, (2001:160)

$$D_h = \frac{d}{1+\frac{2}{\pi}} \tag{8}$$

where d is the diameter of the semicircle. And for a triangular cross-section the hydraulic diameter is defined by Eq. (9) from Hesselgreaves, (2001:158)

$$D_h = \frac{4b}{3} \tag{9}$$

where b is half the perpendicular height of an equilateral triangle.

2.6. Literature survey conclusion

In the literature survey various aspects involving micro-channel research were discussed. Different types of channel geometries were investigated, that lead to the following conclusion: the heat transfer and pressure drop both rises as bends are added to the flow path of channels present in compact heat exchangers. A set of equations that can be used to quantify these two characteristics of micro flow channels was presented in Section 2.2. The boundary conditions that can be implemented when solving the governing equations of energy and momentum conservation were discussed in Section 2.3. The most often used boundary conditions that are implemented in the simulations of flow in micro channels are the constant wall temperature (T) and constant wall heat flux (H2) boundary conditions. The definition for fully developed flow was presented in Section 2.4. The definition of the hydraulic diameters of a semicircular and triangular profile were defined in Section 2.5.

In this study the bend radius, channel path length and channel layout will remain constant while the hydraulic diameter of a semicircular and triangular cross-section trapezoidal channel will be altered to achieve minimum pressure losses compared to a

straight channel. In the next chapter the method used to develop the numerical models will be discussed in detail.

3. CFD models

3.1. CFD Introduction

Versteeg & Malalasekera (2007:1) describe Computational Fluid Dynamics (CFD) as the analysis of different systems involving fluid flow, heat transfer and associated phenomena by means of computer-based simulations. The following is a list of examples of industrial applications that can be simulated with CFD software:

- aerodynamics of vehicles and aircraft (drag and lift)
- hydrodynamics of ships
- energy industry: internal combustion engines and gas turbines
- the flow patterns inside turbo machinery or diffusers
- cooling of circuit boards in electric and electronic engineering
- mixing and separation processes in chemical engineering

CFD is a powerful tool that can be utilised to solve the governing equations of energy, mass and momentum transport using various numerical algorithms. The commercial CFD package STAR-CCM+ was used to simulate the micro-channels of the CHE in this study.

From Munson et al. (2006:193) the three governing equations are defined by Eqns. (10), (11) and (12).

$$\frac{\partial}{\partial t}\int_{CV} \rho \, d\psi + \int_{CS} \rho \mathbf{V} \cdot \hat{\mathbf{n}} \, dA = 0 \tag{10}$$

Where $\hat{\mathbf{n}}$ is the unit vector perpendicular to the control surface (CS) and $\mathbf{V}$ the velocity vector of the mass. In words Eq. (10) states that the rate of change $\left(\frac{\partial}{\partial t}\right)$ of mass inside the control volume (CV) plus the net rate of mass flow through the control surface must equal zero in order to conserve the mass.

$$\frac{\partial}{\partial t}\int_{CV} \mathbf{V}\rho \, d\forall + \int_{CS} \mathbf{V}\rho\mathbf{V} \cdot \hat{\mathbf{n}} \, dA = \sum \mathbf{F}_{content} \tag{11}$$

Where $\mathbf{F}_{content}$ is the forces acting on the contents of the control volume. In words Eq. (11) can be expressed in the following way; in order to conserve the momentum, the change of momentum inside the control volume plus the net rate flow of momentum through the control surface has to be equal to the summation of all the forces acting on the content of the control volume.

$$\frac{\partial}{\partial t}\int_{CV} e\rho \, d\forall + \int_{CS} e\rho \mathbf{V} \cdot \hat{\mathbf{n}} \, dA = (\dot{Q}_{net\ in} + \dot{W}_{net\ in}) \qquad (12)$$

In words Eq. (12) states that the total stored energy (e) per unit mass is for fluid particles entering, leaving and within the control volume. $\dot{Q}_{net\ in}$ and $\dot{W}_{net\ in}$ are the heat transfer rate and work transfer rate on the contents of the control volume.

In using this finite volume method the three equations mentioned above are discretized by dividing the control volume into a set of small fluid elements. The conservation equations are then applied to each volume element, and the set of resulting algebraic equations are solved numerically by the solver used in STAR-CCM+.

The following section gives some background to the terminology that was used during the development, validation and verification of the simulation models that were used.

3.2. Straight channel simulations

To be able to simulate the flow in a semi-circular channel using STAR-CCM+ the following model, Figure 9, was constructed using the modelling package Solid Works 2008 and then imported into STAR-CCM+. The built-in mesh extruder of STAR-CCM+ was used to develop a flow channel with a length of 200mm, see Figure 10. The extruder meshing model was proposed by De Wet (2010), stating that the extruder meshed models are preferred above complete volume meshed models, because they converge faster and uses less time per iteration, when compared to a complete volume meshed model. The complete volume meshed models form uneven finite volumes while the mesh extruder function extrudes the cross-section surface mesh along the length of the channel to form prismatic volume elements.

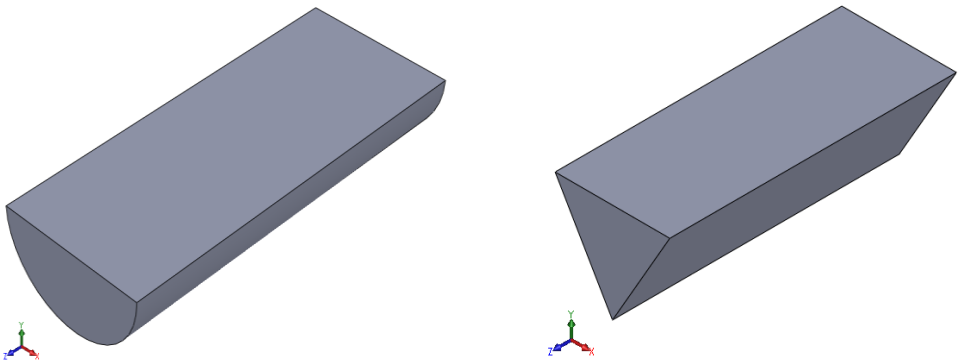

Figure 9 – Solid Works models, Semicircle: D = 2mm, L = 5mm, Equilateral triangle: Sides 2mm, L = 5mm

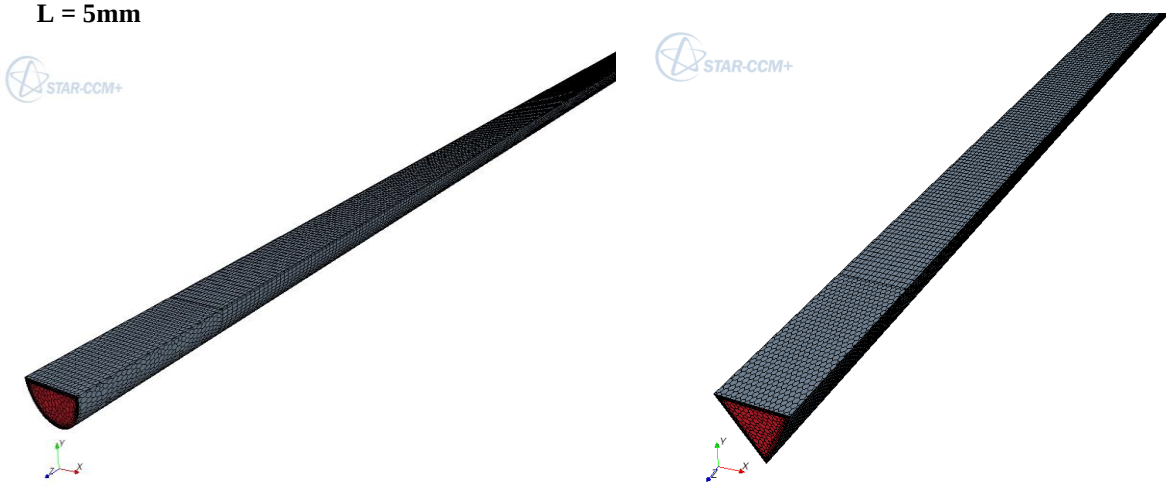

Figure 10 - STAR-CCM+ Extruded models, L = 200mm

The built-in polyhedral meshing tool was used to construct the core mesh and prismatic cells (prism layers) near the walls of the channel. The extruded length of 200mm was enough to ensure that the flow can fully develop thermally and hydro-dynamically.

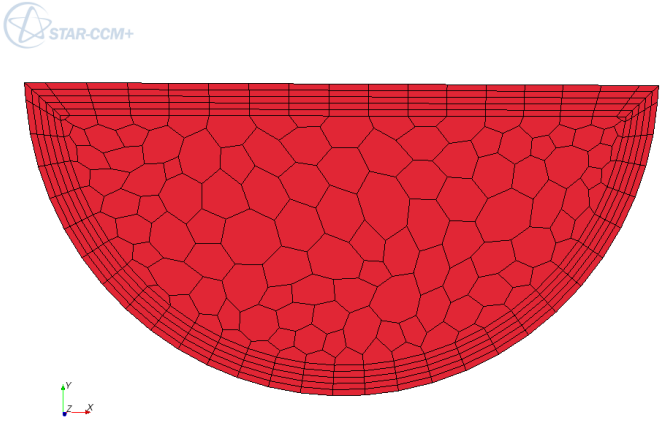

Figure 11 - Inlet face cell distribution for semicircular cross-section with 5 prism layers and 0.15mm core mesh, 361 volume cells on the inlet face

Figures 11 and 12 represent the inlet face cell distribution for the semicircular and triangular cross-sections respectively.

In the case of the semi-circular cross-section the total thickness of the 5 prism layers was 0.1mm, measuring from the wall boundary towards the core mesh in the middle of the channel. The core mesh had a surface size of 0.15mm.

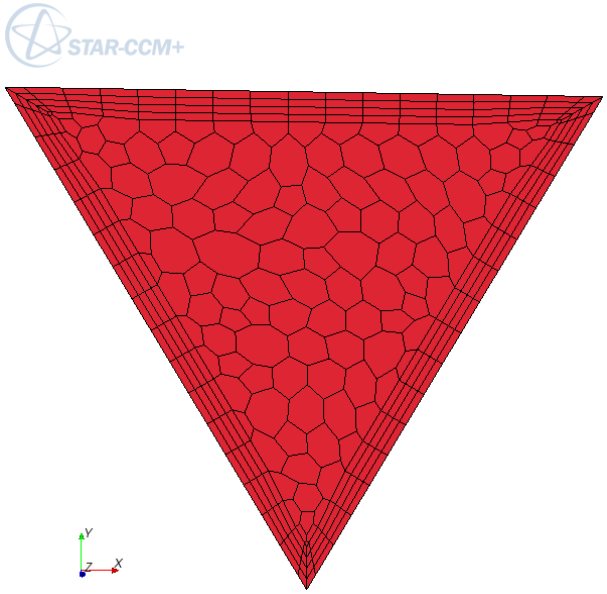

Figure 12 - Inlet face cell distribution for the triangular cross-section with 4 prism layers and 0.15mm core mesh, 328 volume cells on the inlet face

In the case of the triangular cross-section the total thickness of the 4 prism layers was 0.1mm, measuring from the wall boundary towards the core mesh in the middle of the channel. The core mesh had a surface size of 0.15mm.

As stated previously second order segregated flow and –energy solvers were used to solve the governing equations in steady state. The fluid that was used in the simulation was water, with a constant density (ρ), specific heat (C_p), dynamic viscosity (μ) and thermal conductivity (k). The constant wall (T=350K) boundary condition was used at the wall with no-slip. The boundary conditions for the inlet were as follows: a velocity of 0.1469m/s (Re = 200), temperature of 300 K and a pressure of 101325 Pa. At the outlet a ‘flow split outlet’ was specified, with a splitting ratio of 1 (meaning that all inlet flow goes through the outlet boundary). The channels were 200mm in length to allow for fully developed flow conditions.

3.3. Fully developed flow results

3.3.1. Nusselt numbers

According to Shah & London (1978:49) the thermal entry length for fully developed flow is the channel length required so that the local Nusselt number (Nu_x) is 1.05 times the Nusselt number for fully developed flow. The Nusselt number for fully developed flow in a semi-circular cross-section for the constant wall temperature boundary condition is given as 3.323, confirmed by Rosaguti, et al. (2007:697) and Geyer, et al. (2007:3474). Instead of determining a Nusselt number at an arbitrary point in the length of the channel that fits the description given by Shah & London (1978:49) the equation from Kreith & Boehm (1999:4-47) represented by Eq. (6) was used. The Nusselt number was calculated by using the definition from Incropera & De Witt (2005:476)

$$Nu_x = \frac{q_w}{(T_b - T_w)} \frac{D_h}{k} \tag{13}$$

where q_w is the average wall heat flux at a specific axial location in the channel, T_w is the wall temperature and k the thermal conductivity of the fluid. T_b is the bulk mean temperature defined as the mass flow, area averaged temperature, Eq. (14) from Incropera & De Witt (2005:473)

$$T_b = \frac{\int_{A_s} C_p \rho T V_{axial} \, dA_s}{\int_{A_s} C_p \rho V_{axial} \, dA_s} \tag{14}$$

These terms can be moved outside of the integral to be cancelled out mathematically. Eq. (14) then reduces to

$$T_b = \frac{\int_{A_s} T V_{axial} \, dA_s}{\int_{A_s} V_{axial} \, dA_s} \tag{15}$$

where T is the temperature and V_{axial} the velocity in the direction of the flow, perpendicular to the integral of the surface area, A.

The local Nusselt numbers at L_{th} as defined by Eq. (6), are summarised in Table 4, where Nu_x is 3.48915 according to Shah & London (1978:49)

Table 4 - The Nusselt numbers measured for different volume meshes, semicircular cross-section

#	Prism Layers	Core Mesh Size	Volume Cells	Nusselt at L_{th}	Nu_x (T) at L_{th} 3.48915	Asymptotic Nusselt number	Nu (T) 3.323
1	2	0.14mm	213006	3.475544	-0.013606	3.220649	-0.1024
2	5	0.15mm	350514	3.47	-0.01915	3.214861	-0.1081
3	10	0.15mm	557534	3.467494	-0.021656	3.213445	-0.1096
4	15	0.15mm	804549	3.457417	-0.031733	3.213544	-0.1095

Figure 13 shows how the Nusselt number decreases to reach the asymptotic value tabulated in Table 4, for the different mesh resolutions namely: 213006, 350514, 57534 and 804549.

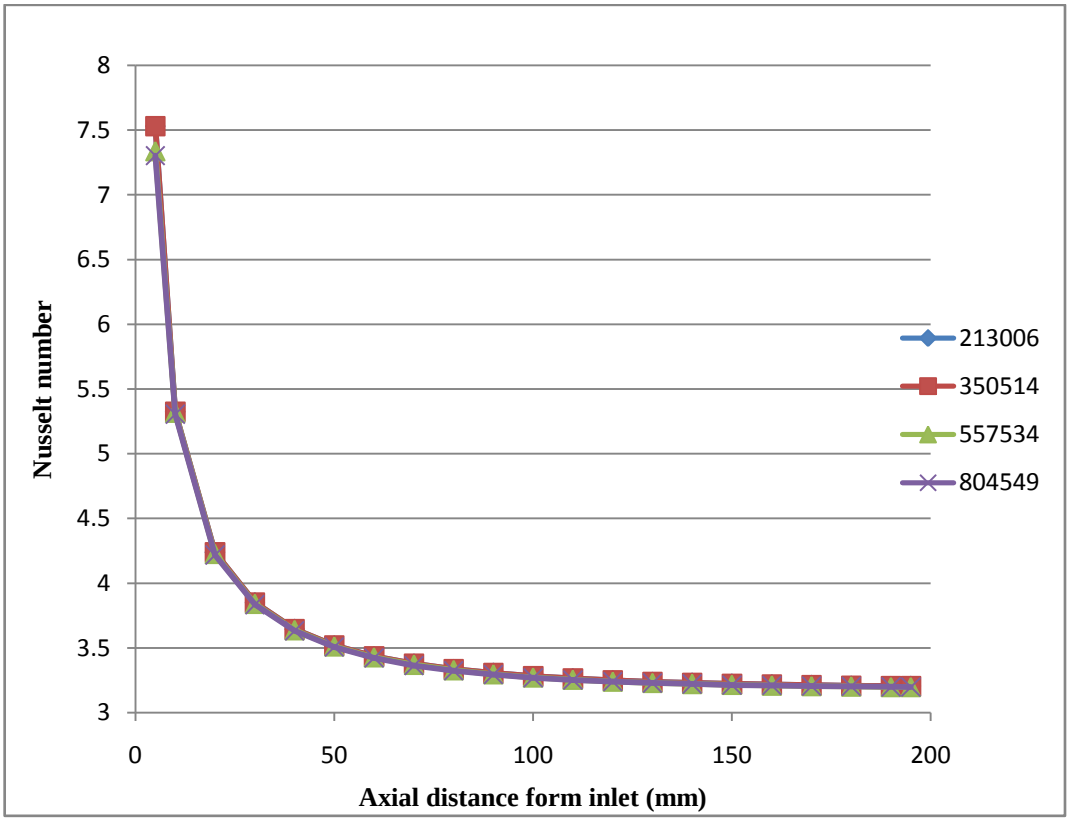

Figure 13 - The Nusselt numbers along the length of the semicircular flow channel

The Nusselt number for fully developed flow in a triangular cross-section for the constant wall temperature boundary condition is given as 2.47, confirmed by Shah & London (1978:224), Incropera & De Witt (2005:496) and Kays & London (1984:120).

Using the definition from Shah & London (1978:49) gives Nu_x as 2.5935. The thermal entry length is calculated as 49.77, by using Eq. (6).

The following table contains the values obtained from the simulation for 4 different models, with increasing number of volume cells.

Table 5 - The Nusselt numbers measured for different volume meshes, triangular cross-section

#	Prism Layers	Core Mesh Size	Volume Cells	Nusselt at L_{th}	Nu_x (T) at L_{th} 2.5935	Asymptotic Nusselt number	Nu (T) 2.47
1	2	0.15mm	231028	2.722049	+0.128549	2.432100	-0.0379
2	4	0.15mm	336298	2.718846	+0.125346	2.426534	-0.0434
3	6	0.15mm	441568	2.717443	+0.123943	2.425396	-0.0446
4	6	0.10mm	541994	2.702796	+0.109296	2.422675	-0.0473

The decreasing Nusselt number along the length of the triangular channel can be seen in Fig. 14 for the different mesh resolutions 231028, 336298, 441568 and 541994.

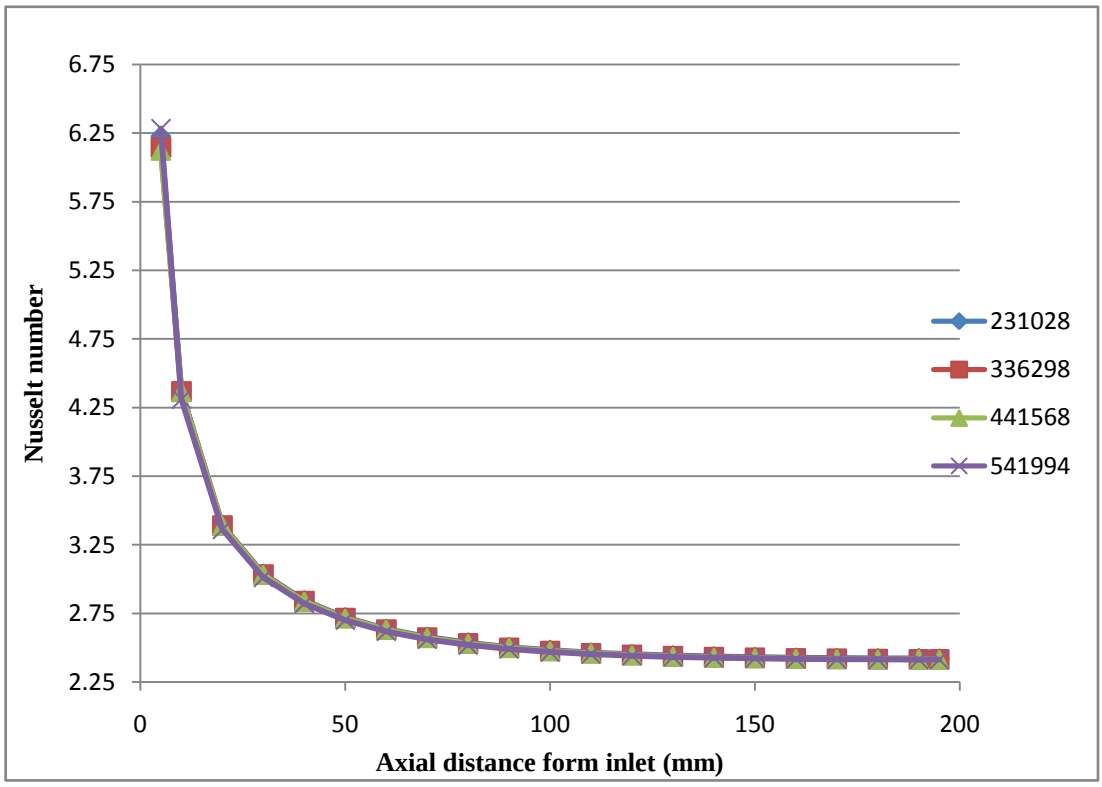

Figure 14 – The Nusselt numbers along the length of the triangular cross-section flow channel

3.3.2. Velocity and temperature profiles

The following figures show the velocity and temperature profile at the thermal entry length L_{th}, for the semi-circular cross-section. All the profiles were extracted at the centre of the diameter of the semicircle or centre of the side of the triangle, perpendicular to the flow.

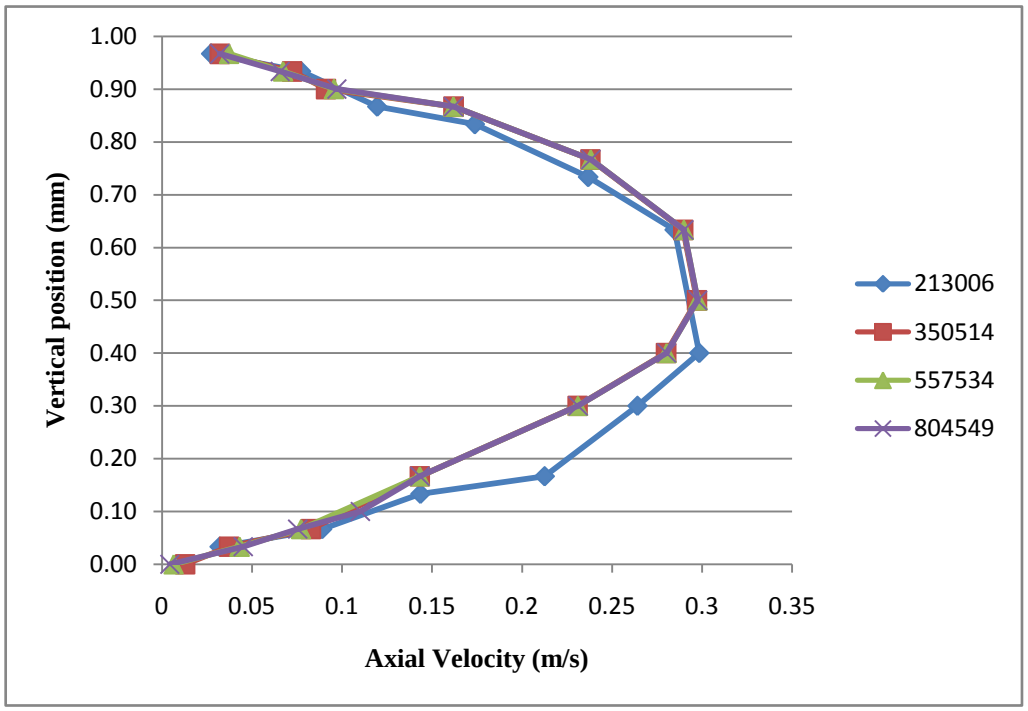

Figure 15 - Velocity profile for different volume mesh resolutions at $L_{th,T}$ = 54.74 mm, semicircular profile

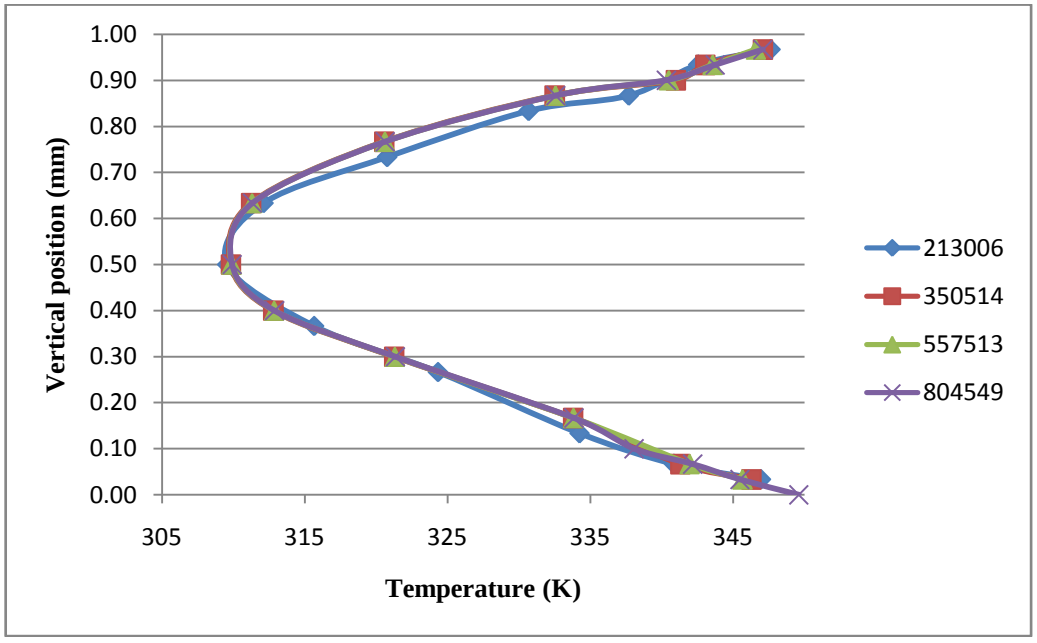

Figure 16 - Temperature profile for different volume mesh resolutions at $L_{th,T}$ = 54.74 mm, semicircular profile

From Figures 15 and 16 it is clear that the solution of the velocity profile and temperature profiles are grid independent from the meshes consisting of 350514 volume cells and finer simulation models. The velocity and temperature profiles for the triangular cross-section are shown in Figures 17 and 18 respectively, for different mesh resolutions. Note that the profiles for the velocity and temperature of the triangular cross-section are grid independent from a resolution of 231028 cells and finer.

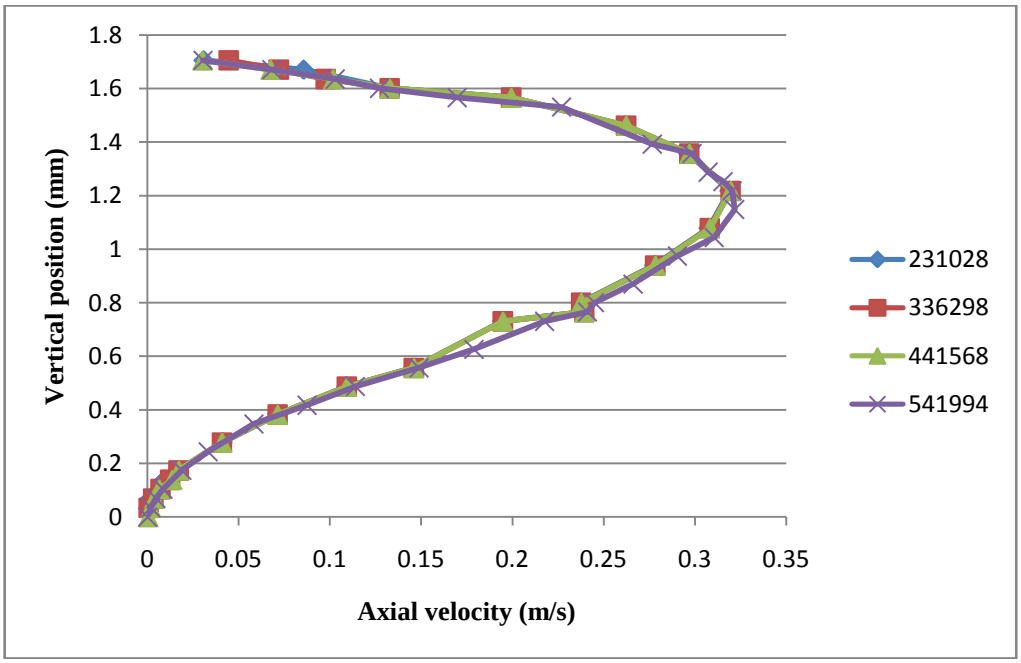

Figure 17 - Velocity profile for different mesh resolutions at $L_{th,T}$ = 49.77 mm, triangular profile

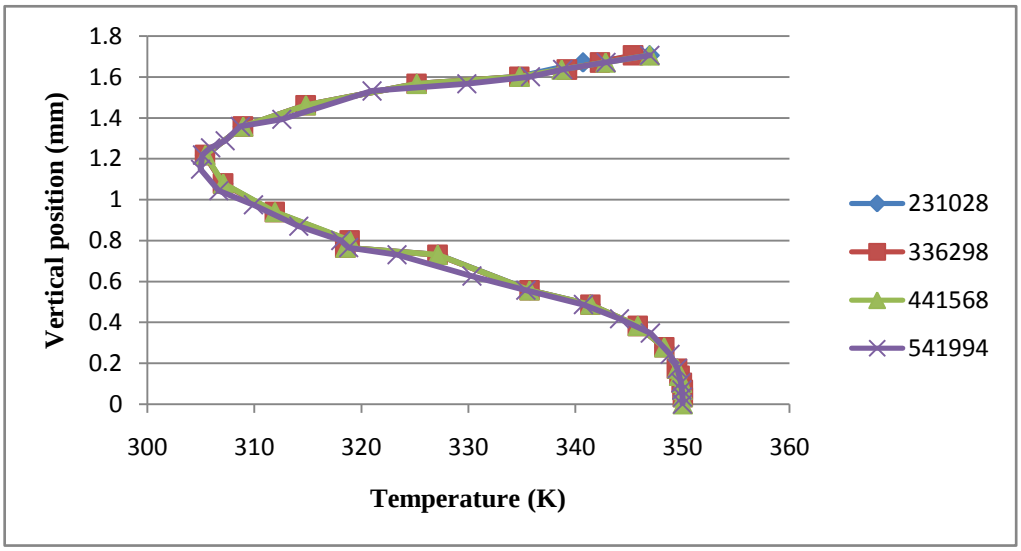

Figure 18 – Temperature profile for different mesh resolutions at $L_{th,T}$ = 49.77 mm, triangular profile

3.3.3. Pressure distribution along the channels

The application of the classical correlations developed for conventional size channels to mini-channels was investigated by Caney et al. (2007:1720). They concluded that the correlations can be applied to mini-channels, since the results of the experiments were in good agreement with analytical solutions regarding heat transfer and pressure drop. Thus in this study the pressure drop over the channels could be compared to the predicted pressure drops using the equation from Munson et al. (2006:413).

$$\Delta p = \frac{1}{2}\frac{f_D}{D_h}\rho V^2 \tag{16}$$

From Eq. (16), f_D is the Darcy friction factor and V the mean axial velocity. The pressure values from the simulations were obtained by applying Eq. (3) at 20mm intervals along the length of the channel. In Figures 19 and 20 the results from the simulation models are compared with the semi-empirical results.

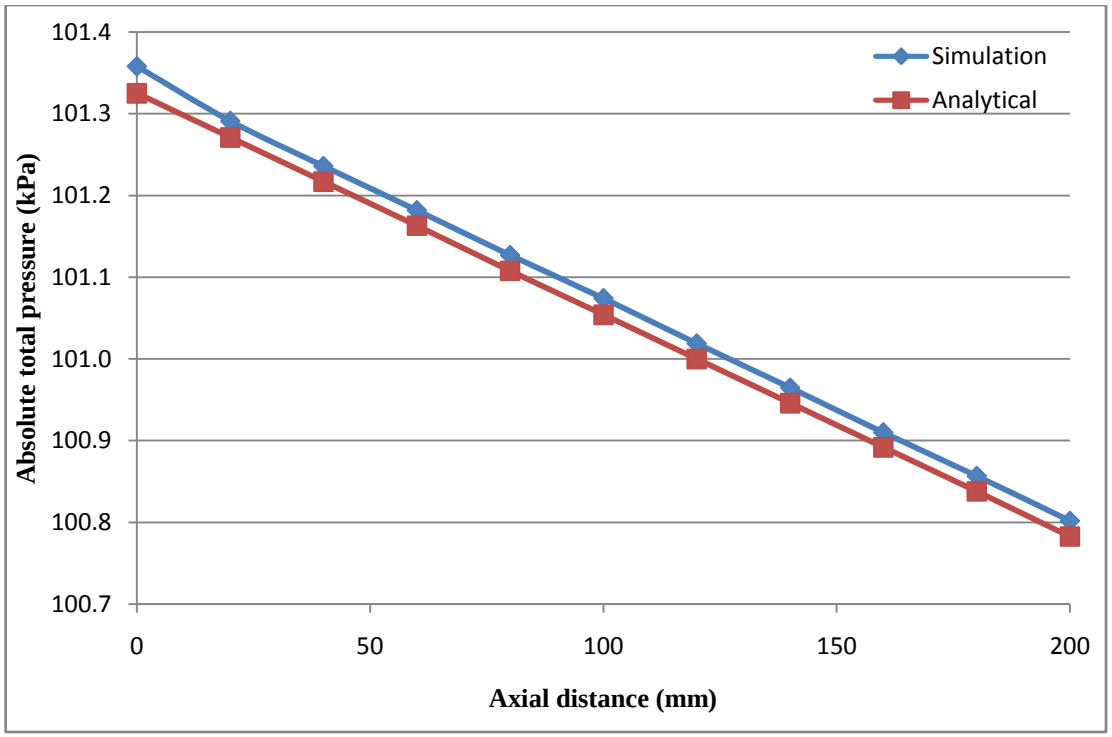

Figure 19 - Analytical and simulated pressure distribution for the semicircular channel profile

From Figure 19 it is seen that the pressure drop from the simulation model is in good agreement with the pressure drop from the analytical solution.

The same approach was used to evaluate the conclusion of Caney et al. (2007:1720), for the triangular cross-section profile.

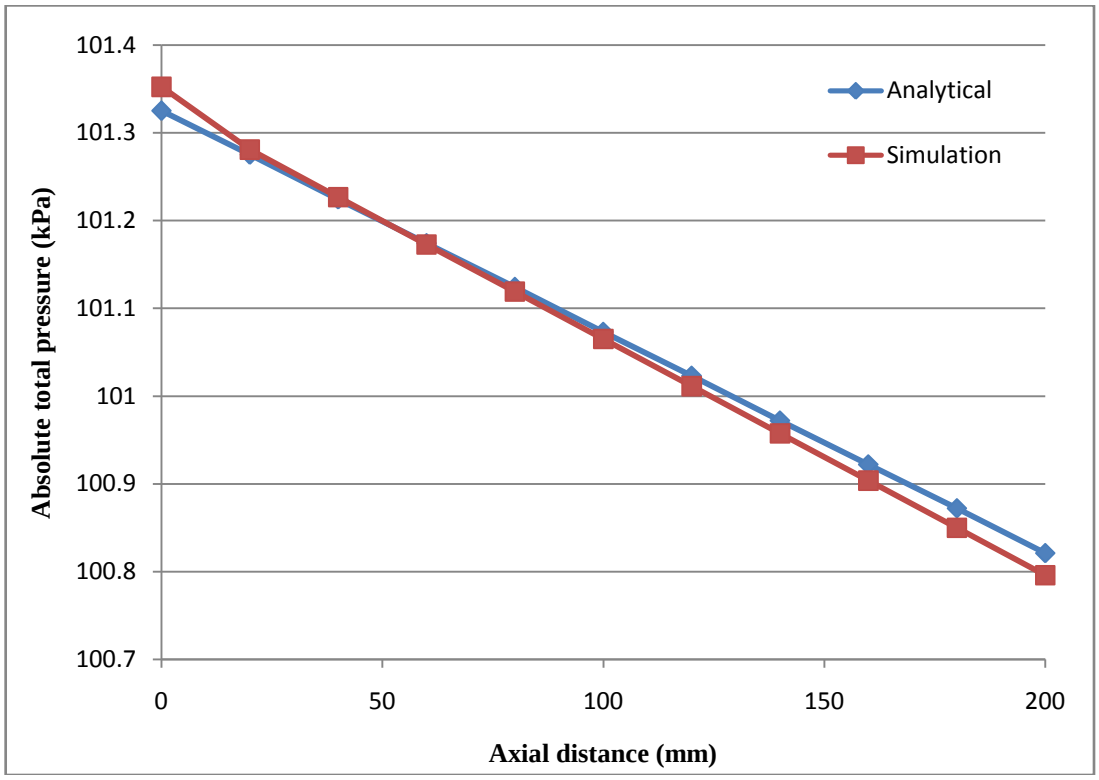

Figure 20 - Analytical and simulated pressure distribution for the triangular channel

The pressure distribution of the simulation is in very good agreement with the pressure distribution calculated using the analytical approach.

3.4 Trapezoidal channel simulations

3.4.1. Simulation model setup

To evaluate the pressure drop over one channel unit of a trapezoidal shaped channel, the method used by Rosaguti et al. (2005:353) and Geyer et al. (2007:3471) was employed. This method involved three consecutive trapezoidal sections being constructed for the numerical model, as shown in Figure 21.

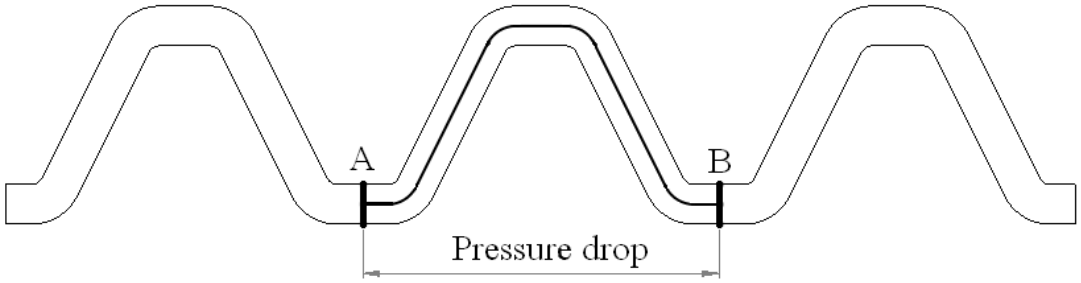

Figure 21 - Three trapezoidal sections

The pressure drop was then measured over the middle part, by constructing perpendicular planes to the flow direction at points A and B respectively. The absolute total pressure was measured at these points by using Eq. (3), (Rosaguti et al., 2007a:697). The pressure drop was then compared with the values obtained analytically for a straight channel with the same path length, by using Eq. (13), (Caney et al., 2007:1715). The path length is the length of the bold line in Figure 21, connecting point A and B by following the centre of the channel along the bends. The method of cyclic sections was proposed by Geyer et al. (2007:3471) and Rosaguti et al. (2005:353) and was used to ensure that fully developed flow conditions are obtained in the middle part.

Trapezoidal channel simulations were done with semicircular and triangular cross-sections by Geyer et al. (2007:3471) and Gupta et al. (2008:2925). Table 6 summarizes the geometric parameters of those studies, and includes the parameters that were used in the current study. Refer to Figure 5 for the definition of the symbols used in the table.

Table 6 - Geometry parameters of this study compared to other geometry parameters for the trapezoidal channel

Gupta, et al. (2007:3471)	Geyer, et al. (2008:2927)	Current study
Semi-circular cross-section	Triangular cross-section	Semi-circular and triangular
$0 \leq Re \leq 200$	$Re = 200$	$25 \leq Re \leq 200$
$R_c/c = 1$	$0.525 \leq R_c/d \leq 1.3$	$R_c/d = 1$
$L/d = 4.5$	$3.6 \leq L/d \leq 12$	$3 \leq L/d \leq 9$
$0 \leq B/L \leq 1.2$	$0.17 \leq B/L \leq 1$	$B/L = 0.5$
$A/L = 0.5$	$0.125 \leq A/L \leq 1$	$A/L = 0.5$

3.4.2. Meshing model validation

The trapezoidal channels were simulated using the same boundary conditions as specified for the straight channels. In the study done by Rosaguti et al. (2006:2914) a swept hexahedral mesh was used for the purpose of computational efficiency. The mesh can be seen in Figure 22.

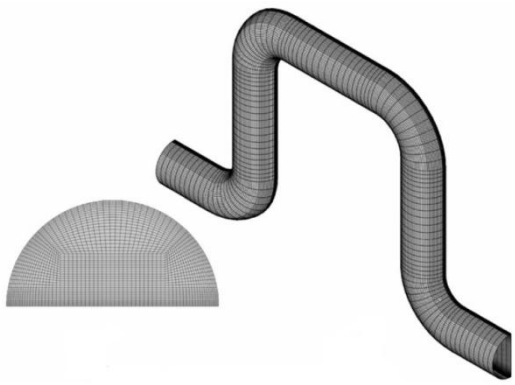

Figure 22 - Mesh density on a cross-section (left) and extruded along the trapezoidal path, Rosaguti et al. (2006:2915)

Unfortunately due to software limitations STAR-CCM+ can only extrude a mesh along a serpentine path if the cross-section of the channel has no sharp edges. Both the semicircle and triangular cross-sections have sharp edges. The meshing of the trapezoidal models were done by using a polyhedral meshing structure for the trapezoidal channel instead of a mesh extruder, see Figure 23.

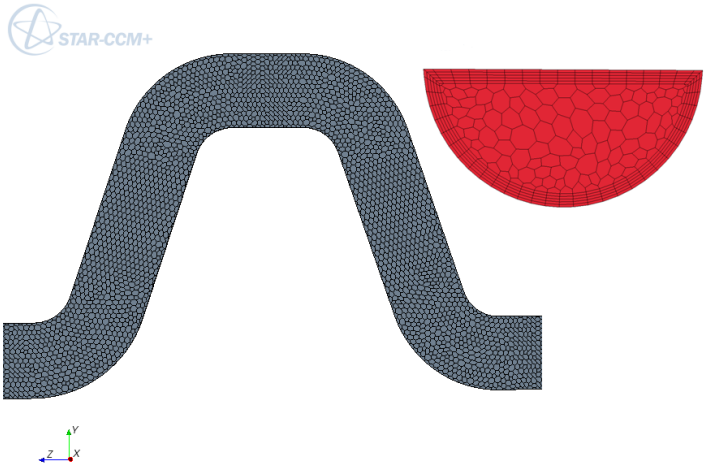

Figure 23 - Polyhedral mesh (left), cross-section face mesh density (right)

An evaluation was done to determine if the results from the polyhedral mesher were accurate. The pressure drop penalty (e_f) as defined in chapter two, by Eq. (2) was used to determine the pressure drop penalty for the specific geometry also used by Geyer et al. (2007:3474). The results were compared with that of the results of Geyer et al. (2007:3474) for the exact same model geometry. In Figure 5 the model geometry for the model is shown with the following geometric relationships: A/L = 0.5, B/L = 0.5, R_c/d = 0.8 and L/d = 4.5.

The results are compared with the current simulation model and shown in Figure 22 for a semicircular cross-section.

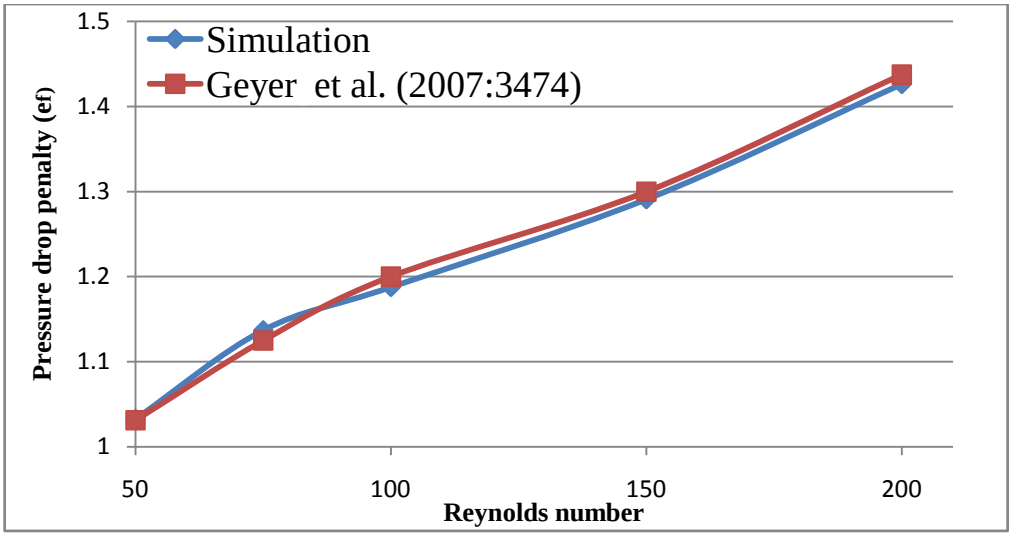

Figure 24 - Comparison of simulation with Geyer et al. (2007:3474), same model geometry

The same was done for the triangular channel to determine if the polyhedral mesh gave sufficiently accurate results. The channel had the following geometric relationships: R_c/d = 1, L/d = 4.5, A/L = 0.5 and B/L = 1. The results is shown in Figure 25.

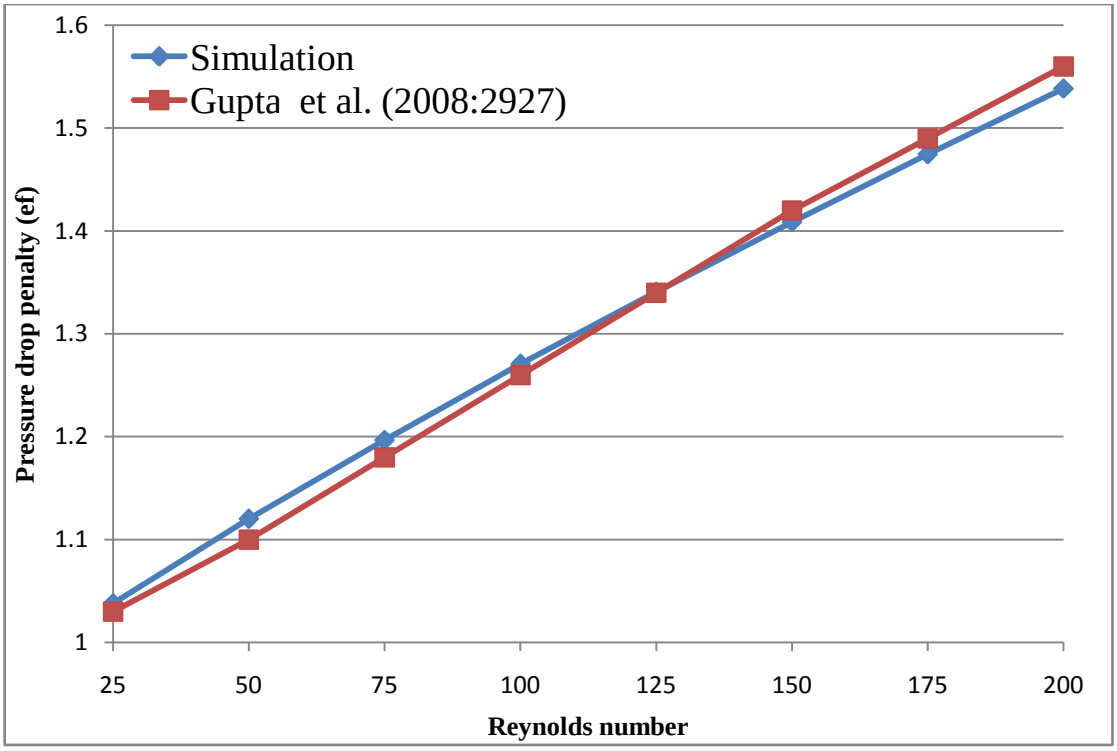

Figure 25 - Comparison of simulation with Gupta et al. (2008:2925), same model geometry

From the evaluation of the meshing model it is clear that the results are in good agreement with values found in literature, thus the polyhedral mesher tool was used to mesh the trapezoidal channels in all the simulation models. The following chapter summarizes the results that were obtained in this study.

4. Results and discussion

The pressure drop penalty was calculated by using the equation defined in chapter two by Eq. 2. The results for the semi-circular cross-section with the varying diameter and the triangular cross-section with a side length equal to the diameter can be seen in Figures 27-31 for Reynolds numbers from 25 to 200. The geometry for these channels were as follows: A/L = 0.5, B/L = 0.5, R_c/d = 0.8 and L/d = 4.5.

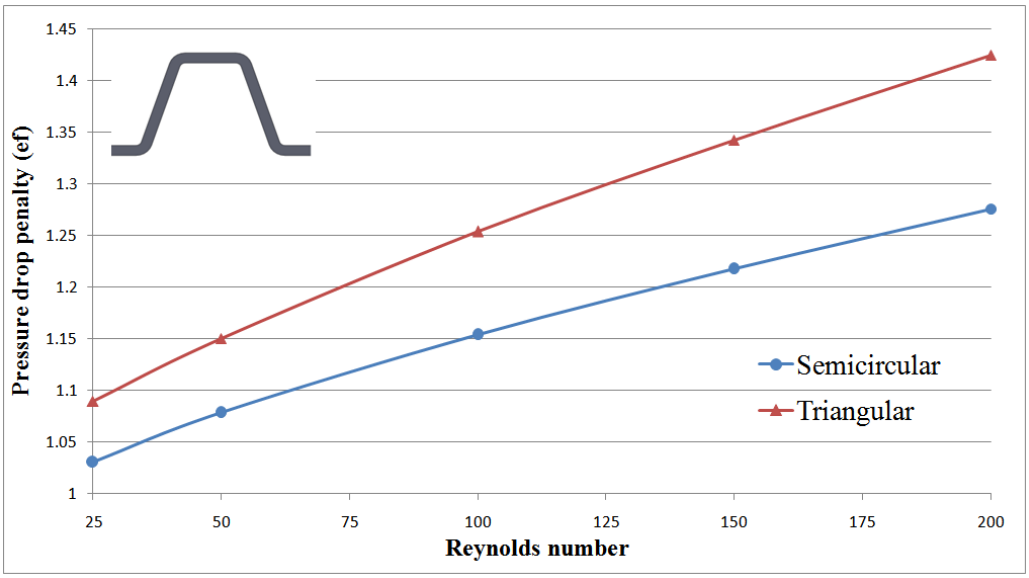

Figure 26 - Pressure drop penalty for both cross-sections with d = 1mm

The pressure drop penalty (e_f) for the triangular cross-section starts at 1.089 for a Reynolds of 25, and increases to 1.15 at Reynolds equal to 50. From there e_f increases linearly to 1.424 for a Reynolds value of 200. The semi-circular pressure drop penalty starts at a value of 1.03 at Reynolds equal to 25, rises steeply to 1.078, then gradually increases as the Reynolds number reaches a value of 200, where e_f reaches a maximum of 1.275, the difference between the maximum pressure drop penalties for the two cases being 0.149 and the difference between the minimum pressure drop penalties for the two cases being 0.059.

The diameter of the semicircle was increased by 50%, to 1.5mm and the results can be seen in Figure 28.

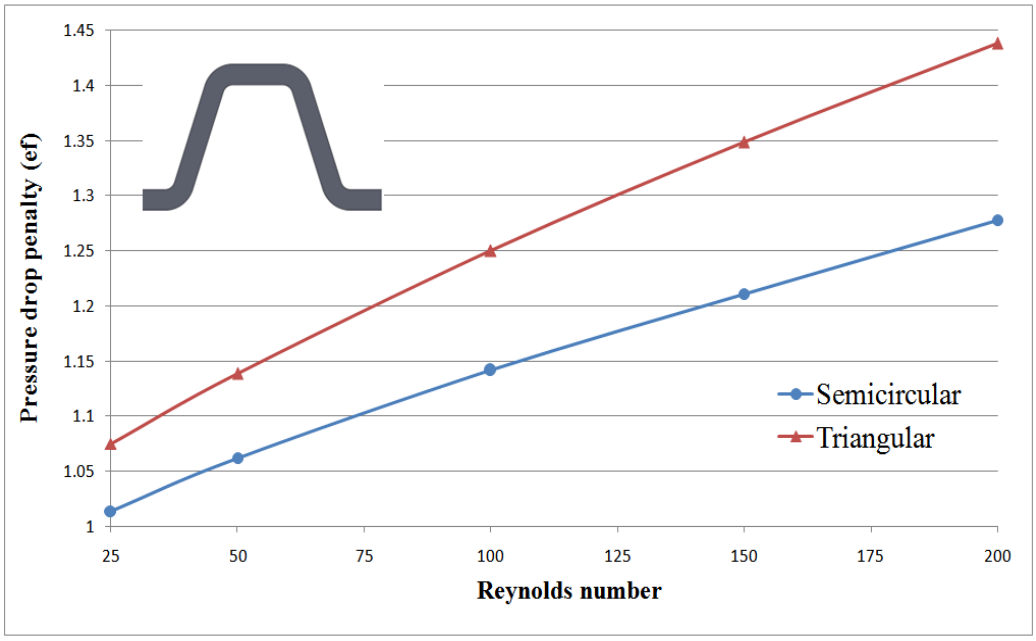

Figure 27 - Pressure drop penalty for both cross-sections with d = 1.5mm

With the Reynolds increasing from 25 to 50, the value for e_f for both cross-sections increases parallel to each other. From there on $e_{f\text{-triangular}}$ increases to a value of 1.44 at Reynolds equal to 200. The value $e_{f\text{-semi-circular}}$ departs from the sharp gradient shared with $e_{f\text{-triangular}}$ and adopts a smoother gradient and attains 1.278 at Reynolds equal to 200.

The following figure shows the comparison between the pressure drop penalty results for the different cross-sections with a diameter of 2mm.

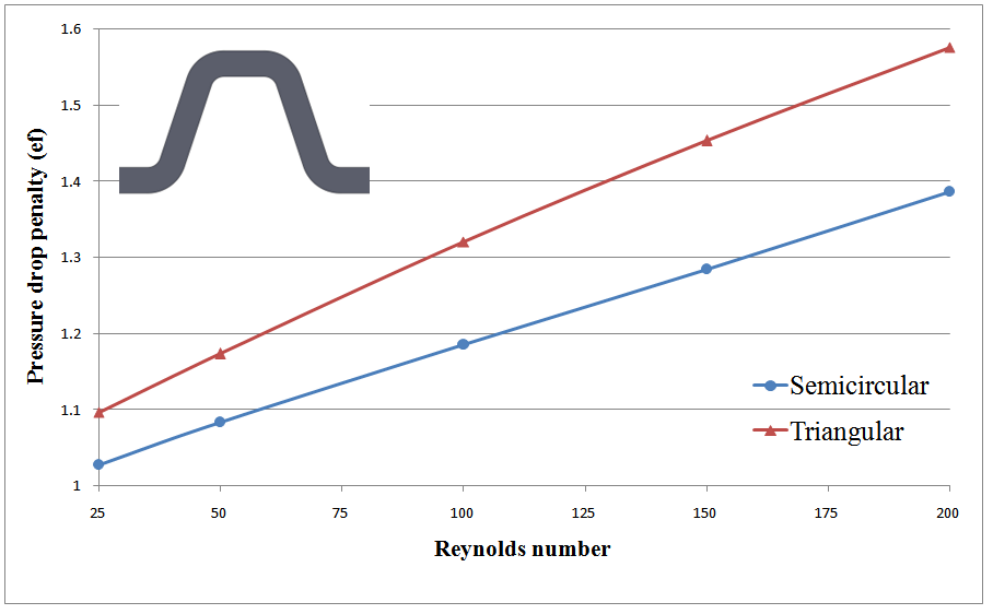

Figure 28 - Pressure drop penalty for both cross-sections with d = 2mm

The pressure drop penalty for the triangular cross-section increases from 1.1 at Reynolds equal to 25 to 1.58 for a Reynolds number equal to 200. This is much higher than the minimum value of 1.027 and maximum value of 1.38 for the semicircular cross-section at the same Reynolds numbers.

The results for the diameter of 2.5mm can be seen in Figure 30.

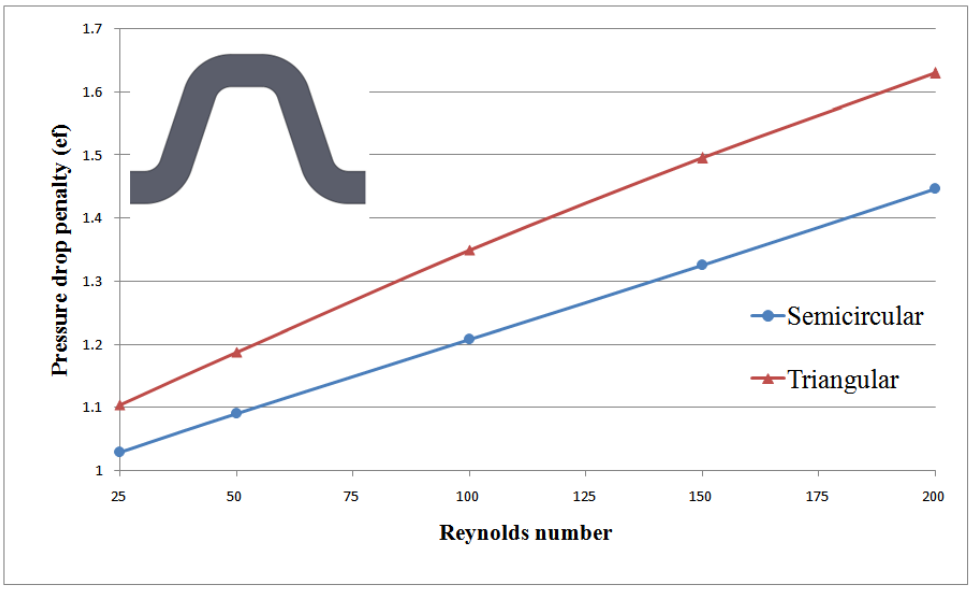

Figure 29 - Pressure drop penalty for both cross-sections with d = 2.5mm

For this larger diameter the two values $e_{f\text{-triangular}}$ and $e_{f\text{-semicircular}}$ almost continues parallel to each other with the increasing Reynolds number. The difference between the values at the Reynolds number equal to 150 is 0.17, and the difference between the values at Reynolds number equal to 200 being 0.183.

The following figure shows the results for the largest diameter used in this study, namely 3mm.

The values for both cross-sections increase with increasing Reynolds number, but at Reynolds between 150 and 200 the value $e_{f\text{-triangular}}$ increases with a slightly sharper gradient than noticed for the Reynolds between 25 and 150. The value $e_{f\text{-semicircular}}$ increases as expected to a maximum value of 1.527 at Reynolds equal to 200 which is 0.228 smaller than the maximum pressure drop penalty value for the triangular cross-section.

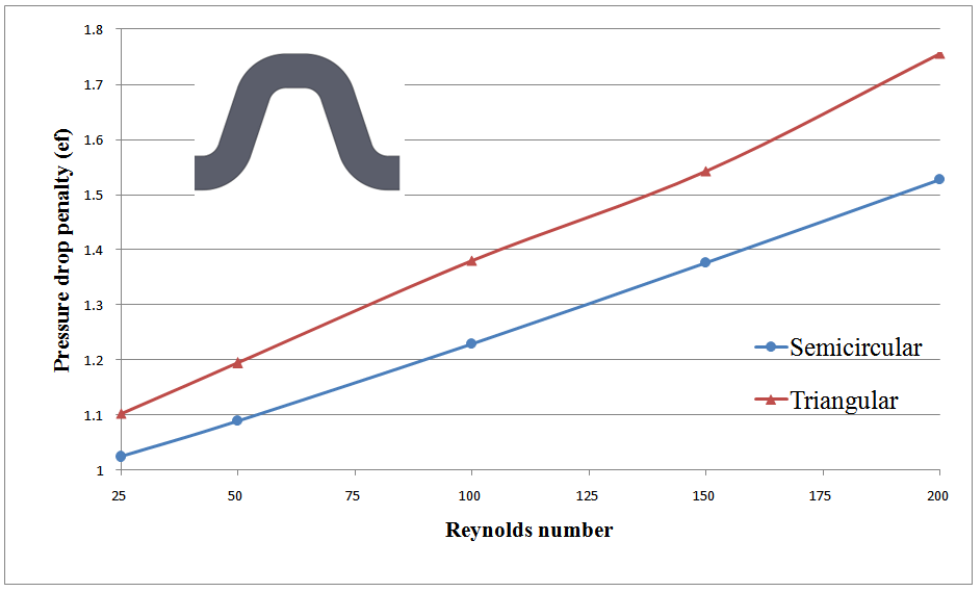

Figure 30 - Pressure drop penalty for both cross-sections with d = 3mm

It is clear from the results that the triangular shaped cross-section has a higher pressure drop penalty than the semi-circular cross-section for all the diameter variations that were considered. Figure 32 and Figure 33 contain the results of all the geometries for the semicircular and triangular shaped cross-sections respectively.

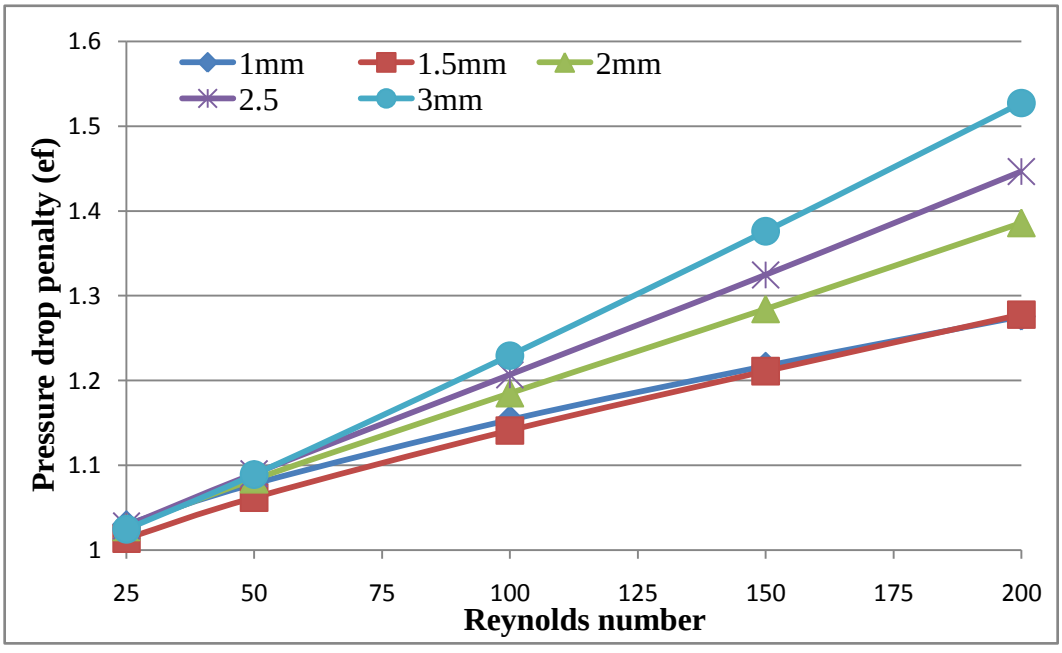

Figure 31 - Pressure drop penalty for the semicircular geometries

The values for the diameters equal to 1mm and 1.5mm are the same at Reynolds numbers equal to 200. Al the starting points for the diameters 2mm to 3mm are close

to 1.03 but fan out with the increase in Reynolds number, reaching different maximum values at the limit of the test range of Reynolds equal to 200.

The triangular geometry variation results can be seen in Figure 33.

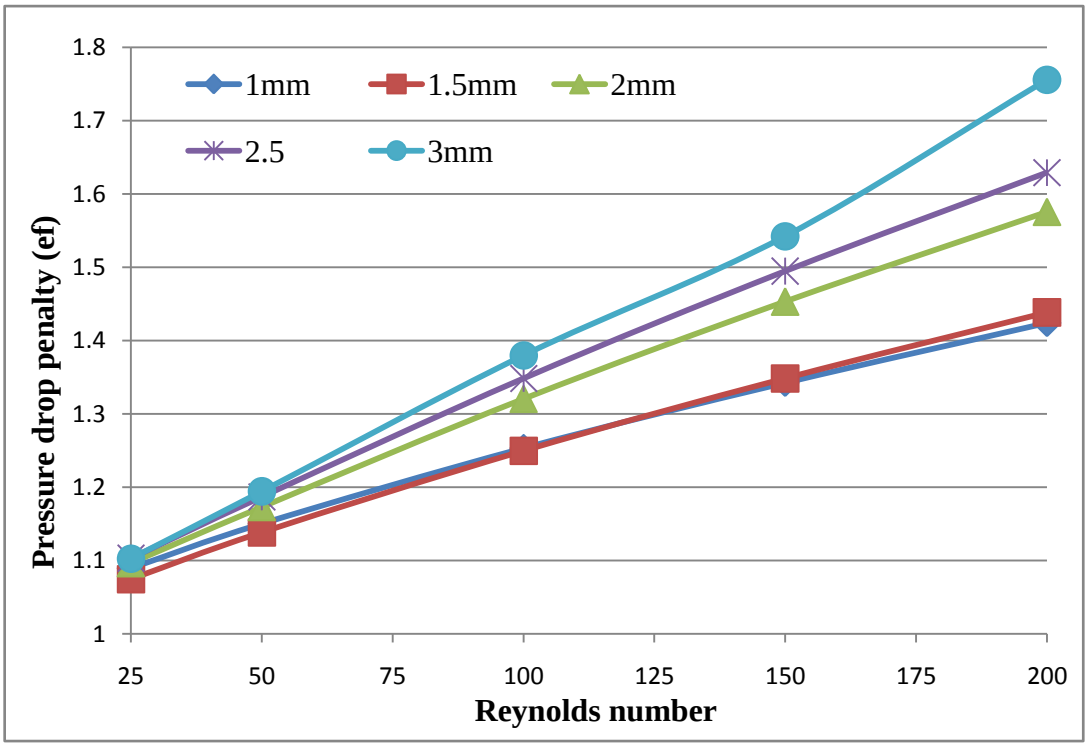

Figure 32 - Pressure drop penalty for the triangular geometries

The values for the 1mm and 1.5mm side length of the triangular cross-section are very close to each for the whole Reynolds range that was used. As in the case of the semi-circular results the triangular pressure drop penalty values start at close to 1.1 for the different side lengths, but fan out with the increase in Reynolds number.

5. Conclusions and recommendations

5.1. Conclusions

From this study it can be concluded that the pressure drop over a trapezoidal channel with semicircular and triangular cross-sections are indeed higher than the pressure drop over a straight channel that follows the same path length.

When comparing the pressure drop penalty of the semicircular cross-section with that of the triangular cross-section, the conclusion is reached that the pressure drop penalty for the triangular cross-section is higher than the pressure drop penalty for the semicircular cross-section with the different geometries considered for each Reynolds number.

From this study it can also be concluded that the optimum hydraulic diameter for a semicircular cross-section with a Reynolds number equal to 200 is 1mm or 1.5mm, because both the diameters have the same pressure drop penalty value at this specific Reynolds number.

From this study it can be concluded that the optimum hydraulic diameter with regards to pressure drop penalty for a triangular cross-section is 1mm for a Reynolds of 200. The pressure drop penalty for the side length of 1.5mm is a little higher than the value for 1mm, but at Reynolds equal to 100 the values are the same.

The recommendations of optimum diameters will also be subject to the provisions that during the overall exchanger design process the target heat transfer and mass flow values can be reached.

5.2. Recommendations

It is recommended to

- expand the design criteria and evaluate the same geometric variations for the triangular and semicircular cross-sections
- investigate the different heat transfer enhancement factors for the same range of Reynolds numbers.
- repeat the study using a different CFD software package (ANSYS) and compare results with the results shown in this study.
- include more cross-sectional shapes in the study for example: trapezoidal and square cross-sections.
- investigate the effect of rounding one or more corners would have on the pressure drop penalty and heat transfer enhancement of the triangular and semi-circular cross-sections.
- use a different solver in the STAR-CCM+ CFD package and compare the results with the results shown in this study.

References

CANEY, N., Marty, P. & Bigot, J. 2007. Friction losses and heat transfer of single-phase flow in a mini-channel. *Applied thermal engineering*, 27:1715-1721.

DE WET, C. 2010. "Private communication" Pretoria.

GEYER, P. E., FLETCHER, D. F. & HAYNES, B. S. 2007. Laminar flow and heat transfer in periodic trapezoidal channel with semi-circular cross-section. *International journal of heat and mass transfer,* 50:3471-3480.

GUPTA, R., FLETCHER, D. F. & HAYNES, B. S. 2008. Thermohydraulic performance of periodic trapeziodal channel with a traingular cross-section. *International Journal of Heat and Mass Transfer*, 51:2925-2929.

GUPTA, R., FLETCHER, D. F. & HAYNES, B. S. 2009. On the CFD modelling of Taylor flow in microchannels. *Chemical engineering science,* 64:2941-2950.

HALLER, D., WOIAS, P. & KOCKMANN, N. 2009. Simulation and experimental investigation of pressure loss and heat transfer in microchannel networks containing bends and T-junctions. *International journal of heat and mass transfer,* 52:2678-2689.

HESSELGREAVES, J. E. 2001. Compact heat exchangers. New York: Elsevier science & technology books. 158-160 p.

IMKE, U. 2004. Porous media simplified simulation of single- and two-phase flow heat transfer in micro-channel heat exchangers. *Chemical engineering journal*, 101:295-302.

INCROPERA, F. & DE WITT, D. 2005. Fundamentals of heat and mass transfer. 5th ed. New York: John Wiley & Sons. 469 p.

KAYS, W. & LONDON, A. 1984. Compact heat exchangers. 3rd ed. New York: McGraw-Hill.

KREITH, F. & BOEHM, R. 1999. Heat and Mass Transfer. Boca Raton: CRC Press LLC.

MUNSON, B., YOUNG, D. & OKIISHI, T. 2006. Fundamentals of fluid mechanics. 5th ed. Hoboken: John Wiley and Sons.

PEI-XUE, J., MING-HONG, F., GUANG-SHU, S. & ZE-PEI, R. 2001. Thermal-hydraulic performance of small scale micro-channel and porous-media heat exchangers. *International journal of mass and heat transfer,* 44:1039-1051.

REAY, D. 2002. Compact heat exchangers, enhancement and heat pumps. *International journal of refrigeration,* 25:460-470.

ROSAGUTI, N. R., FLETCHER, D. F. & HAYNES, B. S. 2005. Laminar flow and heat transfer in periodic serpentine channel. *Chemical engineering and technology, 28*(3):353-361.

ROSAGUTI, N. R., FLETCHER, D. F. & HAYNES, B. S. 2006. Laminar flow and heat transfer in periodic serpentine channel with semicircular cross-section. *International journal of mass and heat transfer,* 49:2912-2923.

ROSAGUTI, N. R., FLETCHER, D. F. & HAYNES, B. S. 2007a. Low-Reynolds number heat transfer enhancement in sinusoidal channels. *Chemical engineering science,* 62:694-702.

ROSAGUTI, N. R., FLETCHER, D. F. & HAYNES, B. S. 2007b. A general implementation of the H1 boundary condition in CFD simulations of heat transfer in swept passages. *International journal of heat and mass transfer*, 50:1833-1842.

ROSENGARTEN, G., COOPER-WHITE, J. & METCALFE, G. 2006. Experimental and analytical study of the effect of contact angle on liquid convective heat transfer in microchannels. *International journal of heat and mass transfer,* 49:4161-4170.

RUSH, T., NEWELL, T. & JACOBI, A. 1999. An experimental study of flow and heat transfer in sinusoidal wavy passages. *International journal of mass and heat transfer,* 42:1541-1553.

SHAH, R.K. & LONDON, A.L. 1978. Laminar flow forced convection in ducts. New York: Academic Press.

VERSTEEG, H. & MALALASEKERA, W. 2007. An introduction to computational fluid dynamics. 2nd ed. Harlow: Pearson Education Limited.